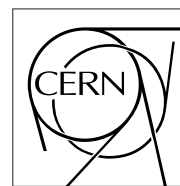**The Compact Muon Solenoid Experiment**

CMS Note

Mailing address: CMS CERN, CH-1211 GENEVA 23, Switzerland

7 July 1998

Test results of the semitransparent amorphous silicon sensors for the link system of CMS

M.G. Fernández, A. Ferrando, M.I. Josa, A. Molinero, J.C. Oller

CIEMAT [a] *, Madrid, Spain*

C.F. Figueroa, N. García, T. Rodrigo, I. Vila

Instituto de Física de Cantabria CSIC-University of Cantabria [b] *, Santander, Spain*

Abstract

Semitransparent amorphous silicon sensors have been proposed as the 2D positioning sensors for the link system of the CMS alignment. We have developed a general method to characterise these sensors, from the signal reconstruction to the beam deflection. The transparency for the HeNe wavelength has also been calculated.

To be submitted to Nucl. Instr. and Methods A

1 Introduction

The semitransparent amorphous silicon sensors were designed to provide position resolutions of the order 1 μm to measure the relative position of particle tracking detectors in a multipoint monitor concept. The original application of these devices was foreseen to fulfil the requirements of the ATLAS [1] alignment system.

Constraints of the same order apply to the CMS [2] alignment . Their special features have also converted the Max Planck Institute (MPI) sensors in the appropriate candidates for the 2D position monitoring in CMS.

In the link system, these sensors provide the linking points in the muon region and in the tracker. In the MABs belonging to the link system, there are two sensors that define the position of the MAB relative to the laser beam. Another four sensors in the tracker ends define the position of the tracker with respect to the laser beam. The Laser Level shares the two sensors of the MAB to provide the ϕ orientation MAB-Tracker.

We have carefully measured the precision in the position reconstruction of a laser beam for one of these sensors. Next, it was used as the sensing detector in transparent mode for the deflection and transmittance measurements. The parametrisation of the sensors obtained here stands just for the tested sensor and cannot be extended for any other sensor. However all Digital Position Sensing Detectors (DPSD) will show the same problems described here and an individual calibration will be necessary before the final assembly in CMS.

Next sections are organised as follows: section 2 describes the main characteristics of the sensors and their expected performances. Then a brief description of the setup and sources used comes in section 3. The reproducibility of linear displacements is reported in section 4 and the beam deflection beyond one sensor is reported in section 5. Sections 6 and 7 introduce the transparency and stability. Finally, summary conclusions are drawn in section 8.

2 The semitransparent amorphous silicon sensors

Semitransparent sensors were first developed by H. KROHA et al. [3] at the MPI. Two different technologies were used in order to produce transparent crystalline and amorphous silicon sensors. Both kind of sensors are multilayer sensors. The crystalline sensors were rejected for alignment purposes. They showed large systematic errors and some resolution degradation near the edges. The strips were built only on one surface spoiling the precision on the transverse coordinate. Besides this, crystalline materials are not resistant to radiation.

In contrast to crystalline silicon sensors, amorphous silicon (aSi) films are fully active and position resolutions of 1 μm have been reported [3]. Sensor layers are designed to be transparent for visible light with a sensitivity of 0.1 A/W at 690 nm and 0.01 A/W at 790 nm. The aSi sensors studied here consist of (see Fig. 1) a layer of hydrogenated amorphous silicon of $\sim 1 \mu$m thickness sandwiched between two layers of $\sim$ 100 nm ITO (indium-tin oxide) electrodes perpendicularly segmented to draw a 2D transparent matrix of 64×64 electrodes. The sensor layers are deposited with Chemical Vapour Deposition (CVD) techniques and segmented using photolithographic methods. The three layers are deposited onto a 0.5 mm thick glass substrate.
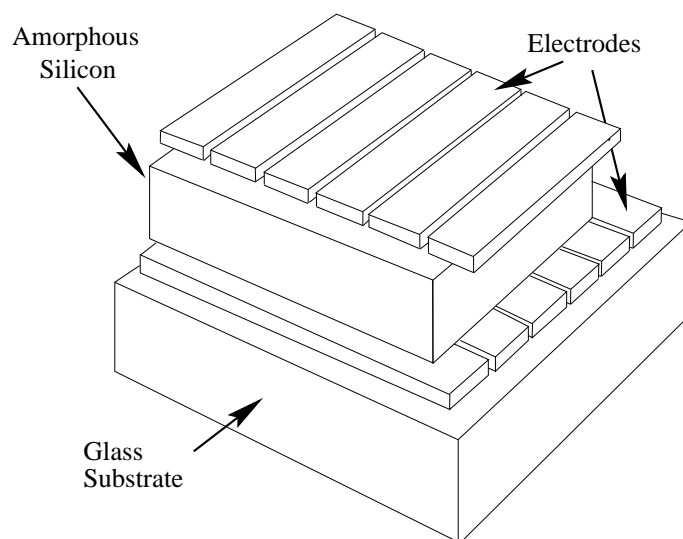

Figure 1: 3D drawing of the layers arrangement in the sensor. The drawing is not scaled.
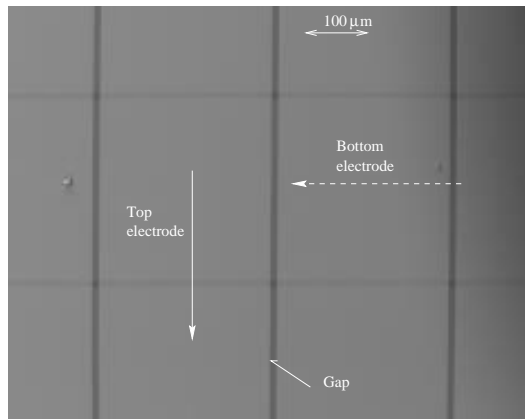
Figure 2: SEM picture of one DPSD sensor.

A scanning electron microscopy (SEM) picture (Fig. 2) of the surface shows the intersections delimited by the small gaps between electrodes. The vertical ones (darker lines in the figure 2) are in the upper layer while the horizontal are two layers underneath. The aSi layer stands between both electrodes. The back and front surfaces of the sensor have different treatments to reflect and absorb, respectively, the red wavelength.

Laser light is partially absorbed by the aSi material, producing photocurrents on the strips. The signal, extracted via gold pads, is multiplexed by 8 multiplexers, converted to voltage and transferred to the ADC of the microcontroller. The most important parameters of these sensors are summarised in Tab. 1.

Table 1: Physical properties of the Silicon strip sensors.

aSi thickness	$\leq 1\ \mu$m
Strips thickness	≤ 100 nm
Glass thickness	500 μm
Number of strips	64 horizontal, 64 vertical
Active area	20 mm $\times$ 20 mm
Size	25 mm $\times$ 25 mm
Strip pitch	312 μm
Strip gap	10 μm

3 Setup

Four DPSDs were purchased to EG&G optoelectronics [4]. The electronics box supplied together with the sensors addresses each sensor and sends the data to a PC. The raw data are transmitted to the PC through the serial port and the readout controlled by a dedicated driver, programmed with LabView [5] and shown in Fig. 3.

Three 20 cm flexible PCB cables are delivered with the equipment, but the distance requirements during deflection measurements between sensors forced us to build two cables of $\sim$3 m and $\sim$6 m.

The laser source employed was a HeNe of 632.8 nm and 3 mW output power. Attenuation filters and a beam expander ($\times$3) focusing at $\sim$1.5 meters conditioned the signal to avoid saturation in the closer sensor and allowed to have a non-negligible intensity in the outer sensor.

During the measurements, the sensors are scanned using horizontal and vertical motorised platforms with submicrometric resolution.

Two different configurations were employed for the tests. The linearity measurements used a laser plus the conditioning optics with one sensor 1.5 meters apart and screwed to two perpendicular motorised platforms. No long cables were used for this experience. For the beam deflection measurements another sensor was added 3 meters downstream the first one. This configuration used 6 meter long cables.
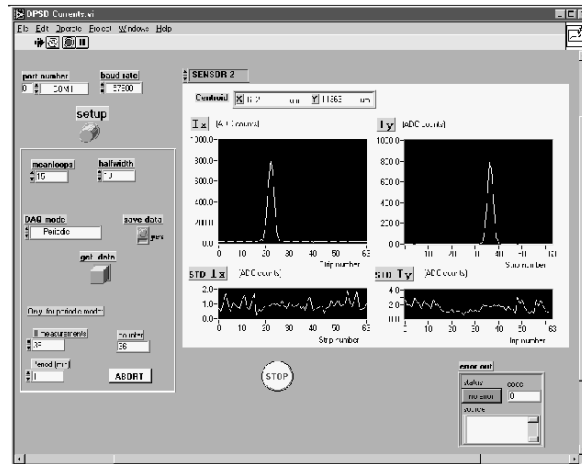
Figure 3: Screenshot of the data acquisition program used. The information of any number of sensors is updated on line. The picture shows the HeNe light used for the test.

3.1 Signal reconstruction

All measurements presented in this work were done in a dark room. During linearity measurements, the signals reconstructed in one sensor were clean Gaussian curves. During the deflection measurements, the signal is spoiled by a tiny background as a consequence of the long cables. A typical signal collected at the bottom sensor of a deflection measurement is shown in Fig. 4.a.
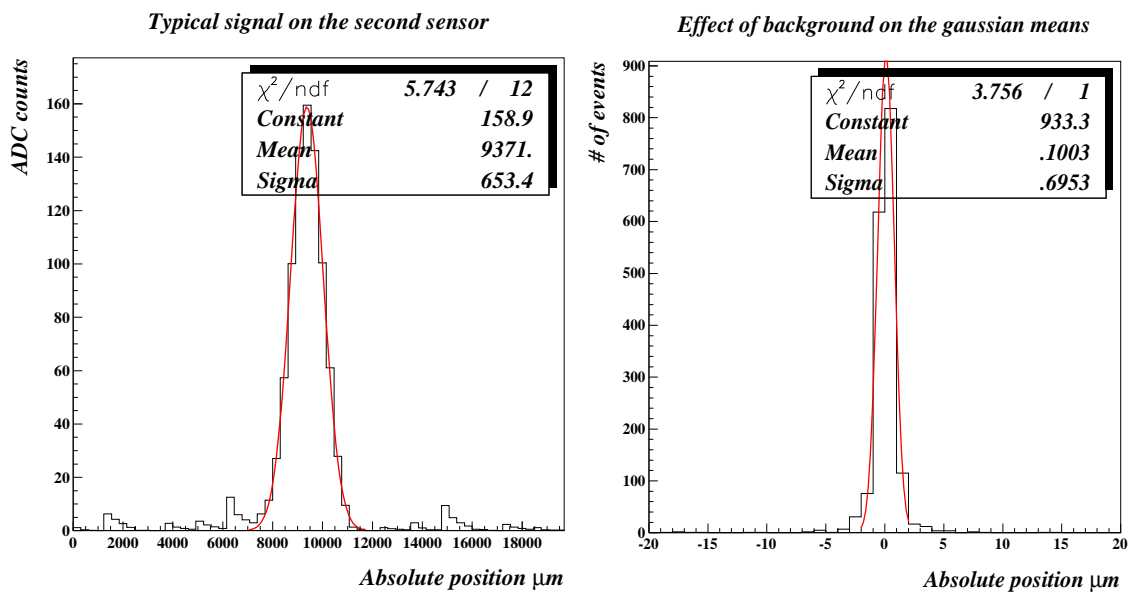

Figure 4: a) Typical signal reconstructed for the HeNe at the bottom sensor . Note the background small peaks produced by the long cables. b) Difference between the Gaussian means fitted with and without the background.

The signal is always fitted to a Gaussian extended ± 7 strips from the maximum. No variation on the mean is observed when the fit extends longer over the tails (see Fig. 4.b). There, the difference in the Gaussian means is shown when the signal is fitted with and without the background. The effect of the background on the fit is negligible.

The data is averaged over 15 measurements and the standard deviation on each strip is used as the weight for the fit. Due to the particular geometry of the electrodes, the information obtained from the incoming beam are two orthogonal intensity profiles.

4

4 Linearity and sensor uniformity

Linearity measurements indicate how well the displacements of the light spot are reconstructed over the sensor. At last, it shows the minimum displacement that the sensor can resolve. During a scan, the difference between the real and the reconstructed displacement allows to know the spatial uniformity of the sensor. The lack of uniformity acts as a systematic error for further measurements.

During horizontal (along X) scans (see Fig. 5) vertical strips give notice on the horizontal displacement while the horizontal strips inform on the parallelism between the axis of the scan and the horizontal axis of the sensors. The equivalent argument stands for a vertical scan. Multiple scans with different motor pitches were taken.
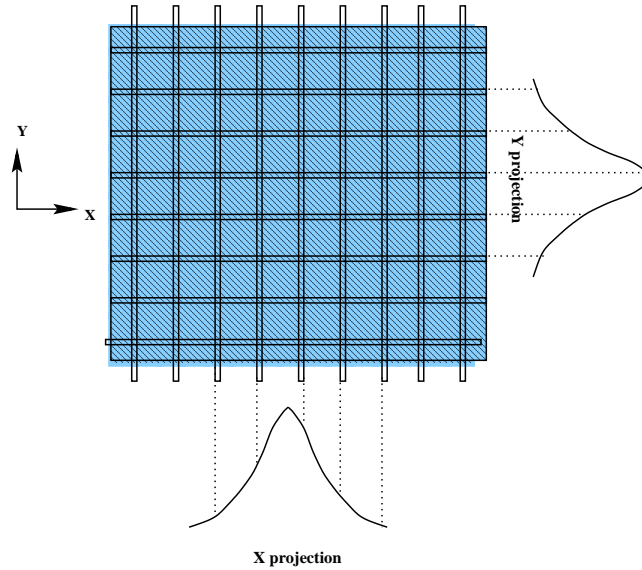

Figure 5: Signal reconstruction in 2D. Horizontal strips integrate the spot giving the Y projection, while vertical strips integrate the signal giving the X projection.

We show in Fig. 6.a, as an example, the linearity observed between real and reconstructed shifts, during a horizontal scan of strip number 31. The small slope showed on the perpendicular projection of the scan (Fig. 6.b) comes from the misalignment between the platform and the sensor horizontal axis. The scan step was 500 μm.

The sensor was swept by the laser beam by means of a motorised platform. Figure 7 shows the residuals of an horizontal linear fit for both sensor coordinates. It is clear that the residuals distribute following a certain pattern.We found that this pattern was not produced by the laser source. We verified it using a laser diode source. The pattern was different for the horizontal and for the vertical projections of the same scan. Different patterns were obtained when the sensor was scanned at different heights. Besides this, the patterns were stable enough to be retrieved when the scan was repeated back and forth under different scanning steps. To illustrate this point we show in Fig. 8 the residuals found in the corresponding linear fits for two other steps: 200 μm (full circles) and 312 μm (stars).

All these evidences together (independence from laser light, independence from platform step) confirm that the existence of a *spatial profile* in the linearity residuals is an inherent characteristic to the sensor. This conclusion agrees with a recent study carried out by Kroha et al. [6] where the spatial profiles are identified with sensitivity variations due to aSi thickness differences. The possible reason for such variations might be standing waves in plasma of the CVD cavity during the deposition process.

The existence of spatial profiles implies a systematic error in the position reconstruction. If this error is small enough there will not be a large degradation in the precision, and then, a representative value for the detection error can be used for the whole sensor. Otherwise, the sensor has to be carefully parametrised, tabulating the sensor inhomogeneities in a 2D grid where the distances between nodes have to be smaller than the period of the spatial profile.

Three horizontal and three vertical lines on two different sensors were scanned. The residuals distribution width amounted ∼5 μm in RMS for the worse of the sensors (see Tab. 2). We took this value as the characteristic detection error for both. If precisions below 5-6 μm are needed then a parametrisation of the whole sensor should be performed.
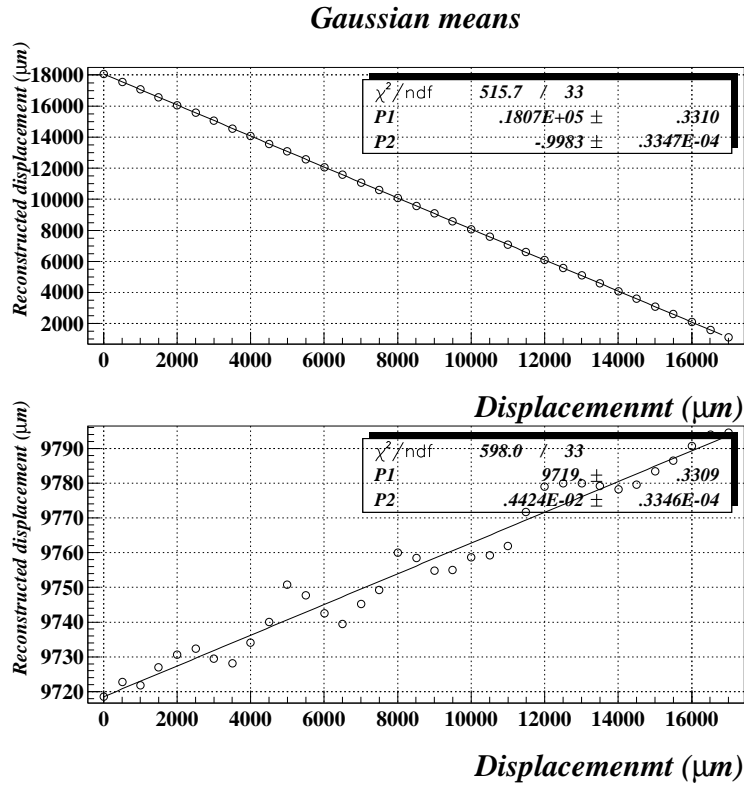
5

Gaussian means

Figure 6: (a) Reconstructed position versus displacement of the platform. (b) Small vertical drift on the horizontal scan.

Table 2: Residuals width for two different sensors. The width is calculated from the Gaussian distribution of the residuals using three single horizontal and three single vertical scans on each sensor.

Sensor	Global (μm)
A	4.6
E	3.9

4.1 Correction of the detection pattern

To find the best grid pitch three horizontal and three vertical lines on the sensors were scanned in steps of 200, 312 and 500 μm (total 18 scans). Then the three scans of 200 μm were first corrected using the information of the scan of 312 μm and then with the scan of 500 μm. Fig. 9.a summarises the residuals width improvement of the 200 μm scans using the 312 μm grid and Fig. 9.b the width improvement using the 500 μm grid for the sensor called A. These results come summarised in Tab. 3.

We found that in order to get 2-3 μm after correction in sensor A, it should be enough to map its inhomogeneity at the level of a 400 μm pitch grid.

The inhomogeneity of sensor G during a 2D scan is shown in fig10. This figure shows its spatial pattern using a grey scale and can be taken as the detection profile of the sensor. The uncorrected residuals width of sensor G amounted to ∼7 μm.

Table 3: Reduction of the RMS after correction of the data by the spatial profile for sensor A. The uncorrected RMS is shown in Tab. 2.

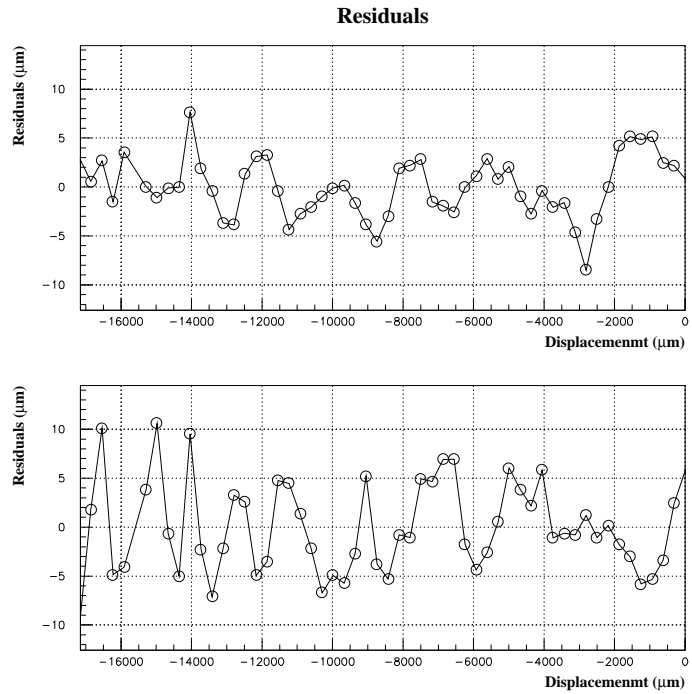| Correction grid (μm)	Corrected residuals width (μm)
312	2.01
500	2.41

6

Residuals

Figure 7: X and Y residuals during a vertical scan of the sensor. The horizontal axis corresponds to the displacement of the motorised platforms. Different patterns are obtained for each coordinate. The RMS of the first plot is 2.7 μm and 4.1 μm for the second.

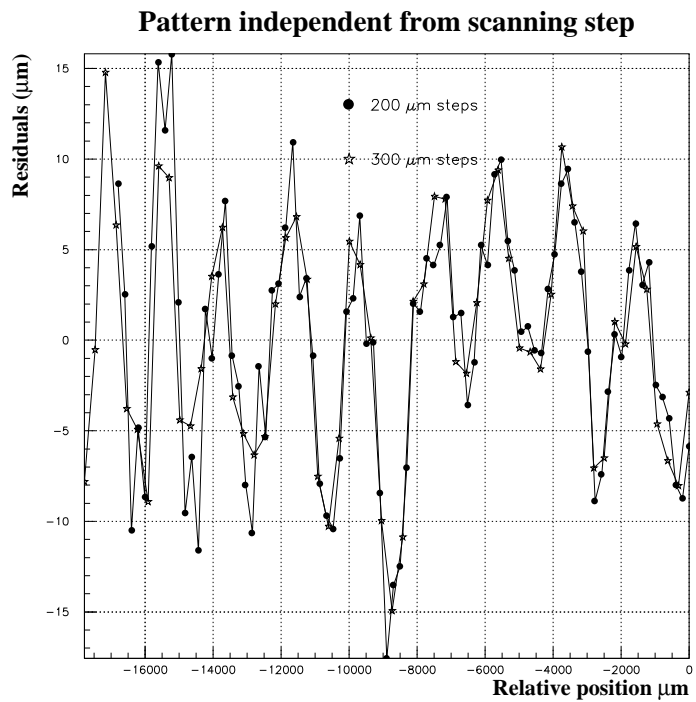**Pattern independent from scanning step**

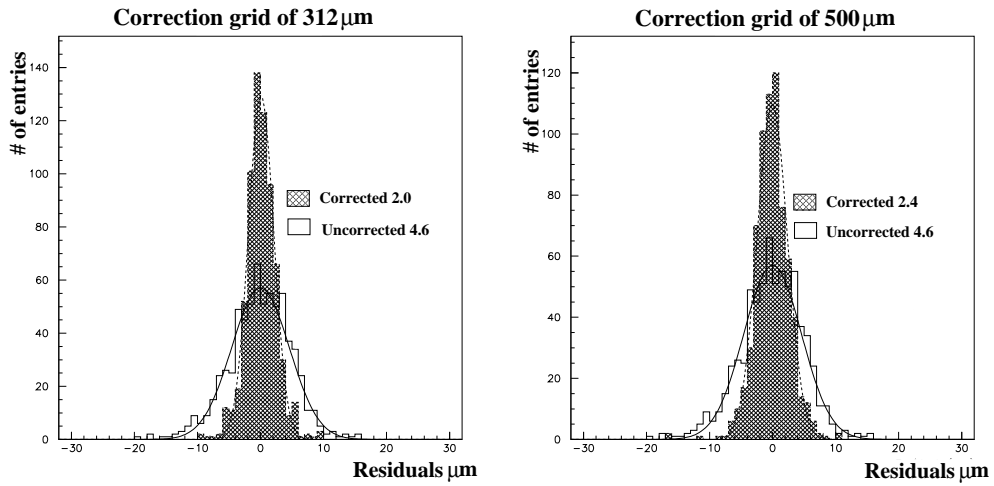Figure 8: The same pattern is reproduced with different scanning steps.

Figure 9: Improvement obtained from a previous knowledge of the sensor inhomogeneity. Three different scan widths are used to map the sensor. The correction improves when the grid width gets narrower.
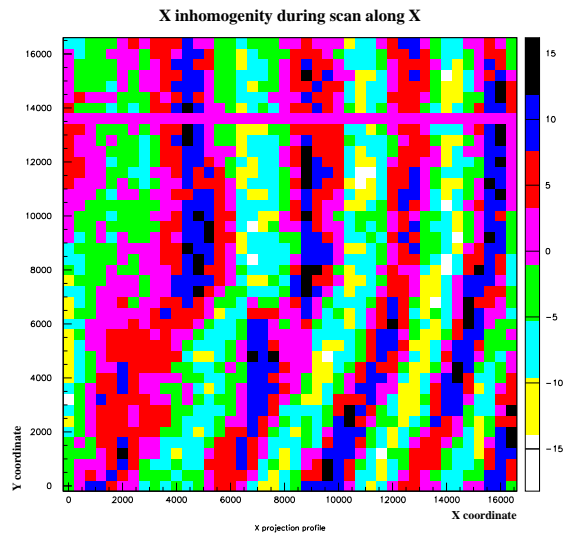

Figure 10: Grey scale plot showing the non uniformity of one sensor. The 80 % of the sensor surface has been scanned with a 400 μm grid width.

5 Beam deflection

When a light ray crosses the interface between two media with different refraction index, the outgoing ray changes its direction with respect to the incoming light direction according to Snell's law. The normal to the surface together with the incident beam define the deflected plane. Due to the 2D layout of the sensor, the deflected light distribution can be decomposed in two projections. From now on, X (Y) deflection means the projection over the vertical (horizontal) strips while the total or global deflection will be the angle obtained combining both projections.

We have studied the beam deflection after one sensor using two DPSDs 3 meters distant on a bench of granite. The undeflected beam is obtained when the first sensor is removed from the light path. Then, it is recovered and scanned with the laser beam. The light profile collected in the second sensor will account for the beam deflection due to the presence of the first sensor. The second sensor is well known, it is the one previously studied (see Fig. 10 and section 4) providing an angular resolution of ≈ 2 μrad, precise enough for the deflection measurements.

The incoming beam going through the DPSD traverses several layers of materials and is deflected by ≈ 30 μrads. During horizontal or vertical scans on the sensor the deflection curves showed all the same tendency (see Fig. 11 as an example). The data distributed with a tiny slope and scattered along it with a sinusoidal-like pattern. Both effects can be explained as follows.
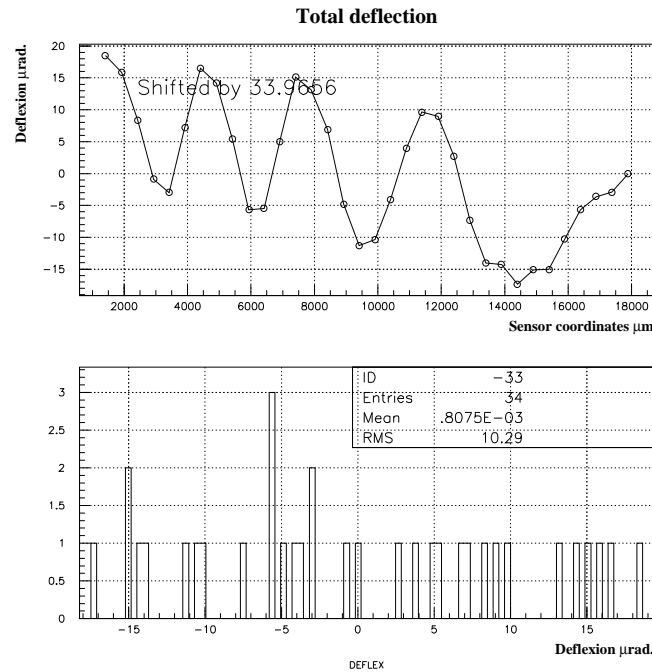

Figure 11: (a) Beam deflection after one DPSD sensor (sensor G). The data have been shifted by 34 μrad to centre around zero. (b) Deflection values projected over the vertical axis. Variations of 20 μrad peak to peak are found.

5.1 Oscillating pattern

The relative dimensions of the DPSD layers make one to expect that the most important contribution to the global deflection will come from the glass substrate because it is the thickest. We associate the deflection pattern on the second sensor as being produced by the glass substrate.

To check this assumption the first sensor is reversed so that the laser beam illuminates the glass surface instead of the ITO and aSi layers (remind the sensor structure from Fig. 1) . After traversing the glass substrate, the light is collected by the layer of aSi of the same sensor. Then, the beam exits and reaches the second sensor, where the deflection is recorded.

Fig. 12 supports this hypothesis, showing that there is a clear correlation between glass inhomogeneity (recorded
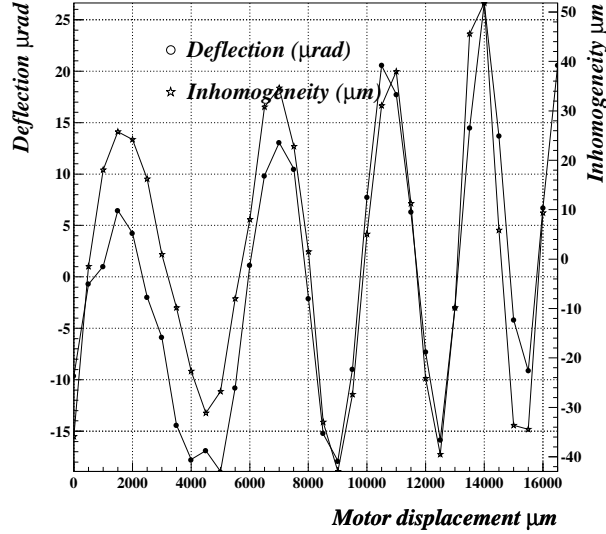
Figure 12: The structure of the first glass substrate is recorded by the first layer of aSi to be compared with the deflection pattern 3 meters away. The left axis is in μrad and the right axis is in μm of inhomogeneity. The deflection curve has been centred around zero to make easy the comparasion.

with the first sensor flipped around) and beam deflection of the first sensor (recorded on the second sensor operating correctly). What we call here "inhomogeneity" are in fact the residuals in a linear fit to the points recorded during a horizontal scan, taken with the sensor flipped around. If the pattern is intended to be explained at all its extent as produced by the substrate orography, the height prominences should amount just hundredth of microns. Light scattering of the laser due to the fluctuations of the refractive index could account for this effect too. We could conclude that the glass substrate produces a beam dispersion/diffusion (inhomogeneity) as well as the oscillating pattern on the deflected data.

5.2   Lens effect

When the light crosses a planoparallel layer, the outgoing beam suffers a translation with respect to the incident point but does not change the original direction. A bunch of incoming parallel rays must shift in the same amount if the layers traversed are good planoparallel films. The shift increases with the layer thickness. Although the beam position changes, the layer, if planoparallel, can not produce a beam deflection because the beam direction keeps unchanged. If the layer is not planoparallel but is a wedge-like, the deflected angle is biased with respect to the incident one by an extra constant quantity depending on the wedge angle and the refraction index.

The slope (Fig. 11.a) on the deflection data might be explained if the wedge angle changes linearly, that is, the surface of the glass is somewhat as a parabola. Therefore, the sensor with this radius of curvature behaves as a lens. In order to have an idea of the contribution to the sagita of the substrate to the slope, we have measured the deflection introduced by a planoparallel layer replacing the first sensor by a planoparallel layer in the two sensors configuration. It was calculated that a sagita of 1 μm in the planoparallel layer leads to the slope observed in Fig. 13. Sagitas of the same order of magnitude in the glass substrate can account for the beam deflection slope.

Independently on the origin of the deflection problem, the absolute value of the deflected angle is too large to be neglected and has to be corrected. We have employed the same method used for the correction of the detection pattern. A full scanning of the sensor is accomplished to evaluate the deflection angle at the nodes of a 42 columns $\times$42 rows sensor calibration matrix. The result of this global scanning is shown in Fig. 14. The unitary cell was a square of 400 μm. The value of the deflection can now be calculated anywhere in the neighbourhood of these nodes by interpolation in the two coordinates. The best interpolating algorithm was chosen extracting subsets of interleaved 21 $\times$42 points of the grid and then reinterpreting the remaining 21$\times$42 points as the new calibration matrix. Briefly, the problem of the 2D interpolation in the removed nodes is broken in two 1D vertical interpolations to the left and right of the unknown node and then another 1D horizontal interpolation using the
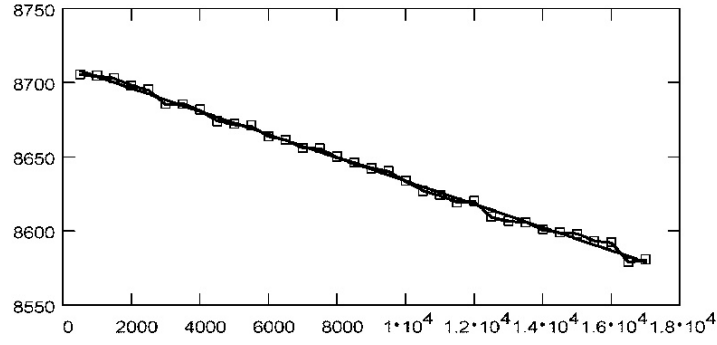
10

Figure 13: Deflexion measured for a planoparallel layer of 18 mm diameter 1.5 meters away from a DPSD. The thickness of the layer produces a global deflection of 86 μrad.
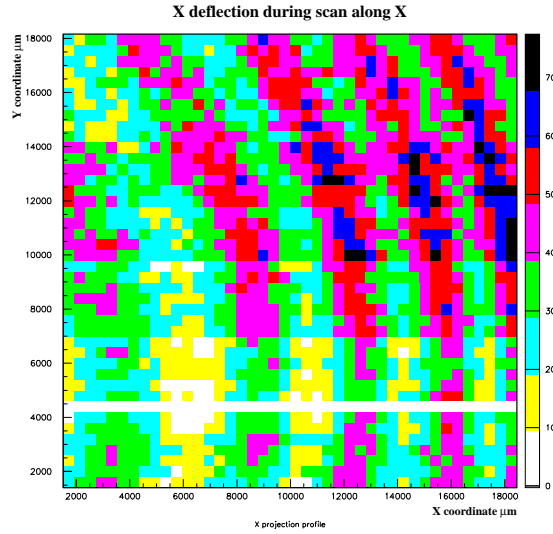

Figure 14: Global deflection matrix with a square unitary cell of 400 μm.

former interpolated values. The unitary cell is now a rectangle of 400 μm$\times$800 μm. In Fig. 15.c it is shown the reduction of the global deflection for the 21 trial scans after correction of the original distribution (Fig. 15.a) by the interpolated value distribution (Fig. 15.b). The correction for both X and Y projections is given in Tab. 4.

6 Transparency

The HeNe wavelength is not the most suitable to operate the DPSD sensors because it is far away from the peak (690 nm) and a poor transmittance is expected. Nevertheless, and for completeness, we have calculated the fraction of light reaching the second sensor in terms of the optical power. This value is easily obtained from the deflection experiments, taking care to focus the beam waist near the middle way of both sensors. We can assume the transmittance ratio to be:

$$\tau(\%) = 100\frac{P_2}{P_1}$$

where P_1 and P_2 are the optical power on both sensors. The value obtained is $(21\pm1)\%$ for both components (see Fig. 16). This low value for the signal on the second sensor is still enough to have a good reconstruction on it. The χ^2 test (see Fig. 17) for the second sensor signal shows that the Gaussian fit to the signal still behaves well spite of the low signal level.
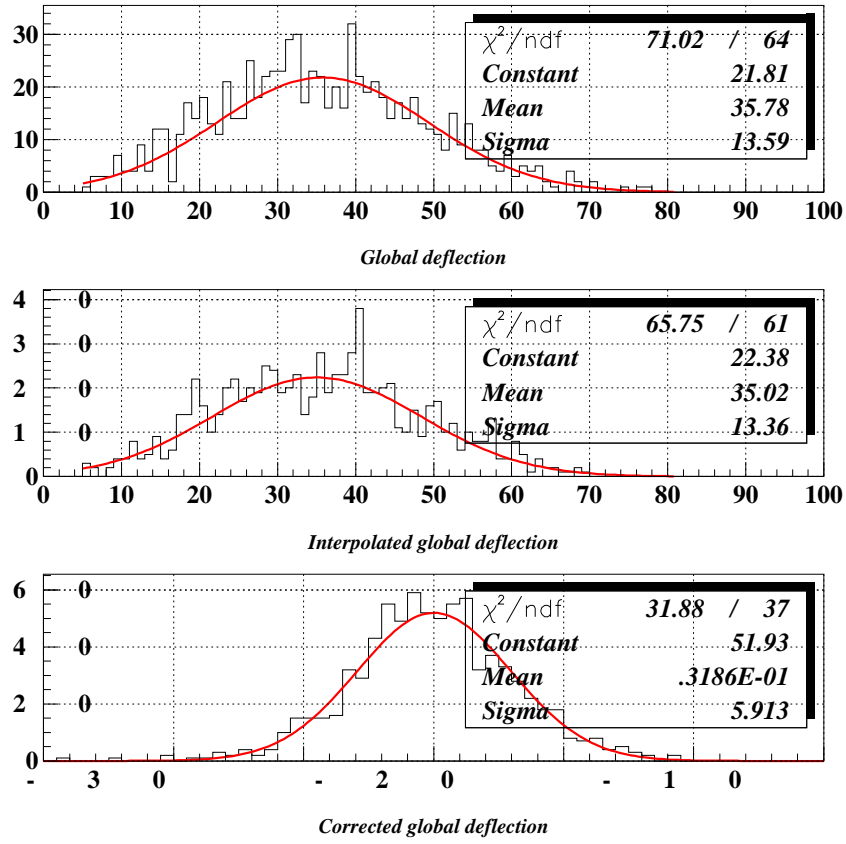
11

Global deflection

Figure 15: Frequency distribution of the trial scans for the: a) Uncorrected distribution; b) Interpolated distribution; c) Corrected distribution.

Table 4: Deflections widths for the raw, interpolated and corrected deflections. All numbers are given in μrad.

Raw data		Interpolated	Corrected
Mean X	34.35	34.62	0.097
σ_x	22.65	12.90	5.887
Mean Y	-4.17	-4.31	-0.1
σ_y	5.78	5.51	2.89
Global Mean	35.78	35.02	0.03186
σ	13.59	13.36	5.91

Transmittance for X and Y

Entries	1722
Mean	21.39
RMS	1.164
UDFLW	.0000E+00
OVFLW	.0000E+00

Transmittance (%)

Entries	1722
Mean	21.55
RMS	1.550
UDFLW	.0000E+00
OVFLW	.0000E+00

Transmittance (%)
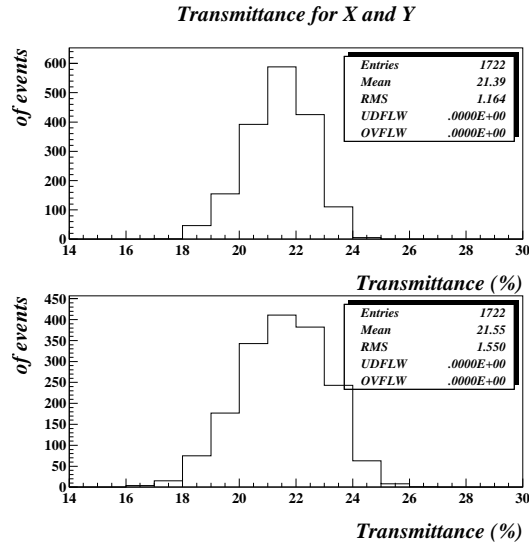
Figure 16: (a) Transmittance for the X coordinate calculated for all the scans showed in Fig. 10 (b) The same for the Y coordinate.

χ^2 **sensor 2**
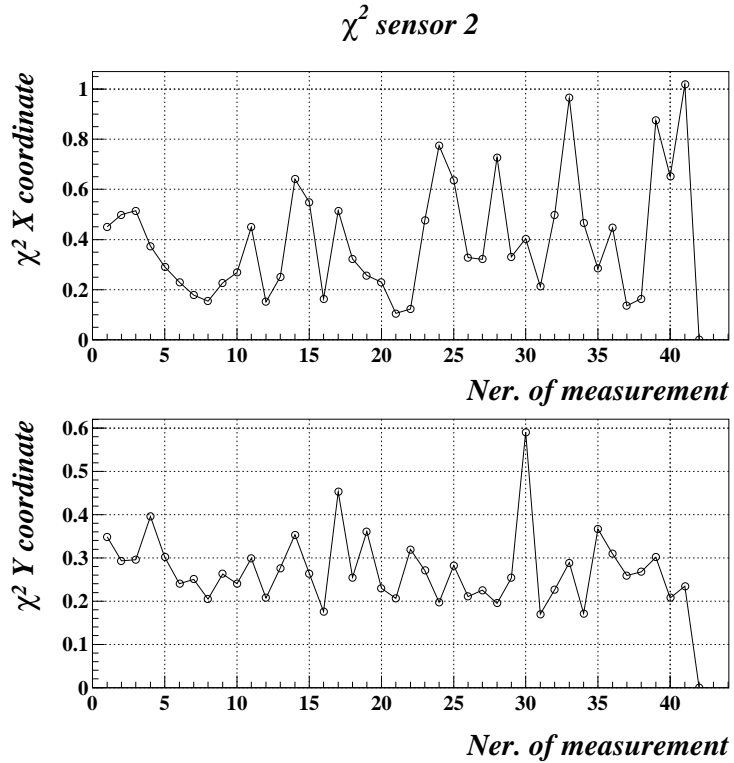
Ner. of measurement

Ner. of measurement

Figure 17: (a)χ^2 value for 42 reconstructions of the signal along a line of the sensor. (b) The same for the perpendicular strips.

13

7   Stability

No long term stability measurements have been taken up to now. These results will be reported in a near future.

8   Conclusions

The detection characteristics of one DPSD sensor using a HeNe have been fully tested. Although the linearity is good, 2D spatial profiles have been observed. The precision obtained gets improved when the sensor profiles are first parametrised and then subtracted, obtaining resolutions of order 3 μm after corrections.

Regarding the beam deflection, we have related the origin of the deflection pattern with the glass substrate of the crossed sensor. The average deflection value of $\approx$30 μrad has been suppressed and the original variations of 14 μrad have been reduced down to 6 μrad using an asymmetric 400 $\times$ 800 μm grid matrix. We expect to improve these values using the whole 400 $\times$ 400 μm over future measurements.

References

[1] **ATLAS Techinal Proposal**. CERN/LHCC/94-43, LHCC/P2 15 December 1994.

[2] **CMS Technical Proposal**. The CMS Collaboration, CERN/LHCC 94-38, LHCC/P1,December 1994

[3] **Nucl. Instr. and Meth. A367 (1995) 413**, W. Blum, H. Kroha, P. Widmann

[4] EG&G Optoelectronics, 45 William Street, Wellesley, Massachusetts, 02181 U.S.A.

[5] LabVIEW, National Instruments Corporation.

[6] **Nuclear Physics B (Proc. Suppl.) 54 B (1997) 80-85** Laser-alignment system with transparent silicon strip sensors and its applications. H. Kroha